Identification of a stereotypic molecular arrangement of endogenous glycine receptors at spinal cord synapses

Stephanie A Maynard[1], Philippe Rostaing[1], Natascha Schaefer[2], Olivier Gemin[1], Adrien Candat[1], Andréa Dumoulin[1], Carmen Villmann[2], Antoine Triller[1]*, Christian G Specht[1,3]*

[1] Institut de Biologie de l'ENS (IBENS), Ecole Normale Supérieure, CNRS, Inserm, Université PSL, Paris, France

[2]Institute for Clinical Neurobiology, University Hospital, Julius-Maximilians-University, Würzburg, Germany

[3]Diseases and Hormones of the Nervous System (DHNS), Inserm, Université Paris-Saclay, Le Kremlin-Bicêtre, Paris, France

* correspondence: christian.specht@inserm.fr, triller@biologie.ens.fr

Supplementary Information

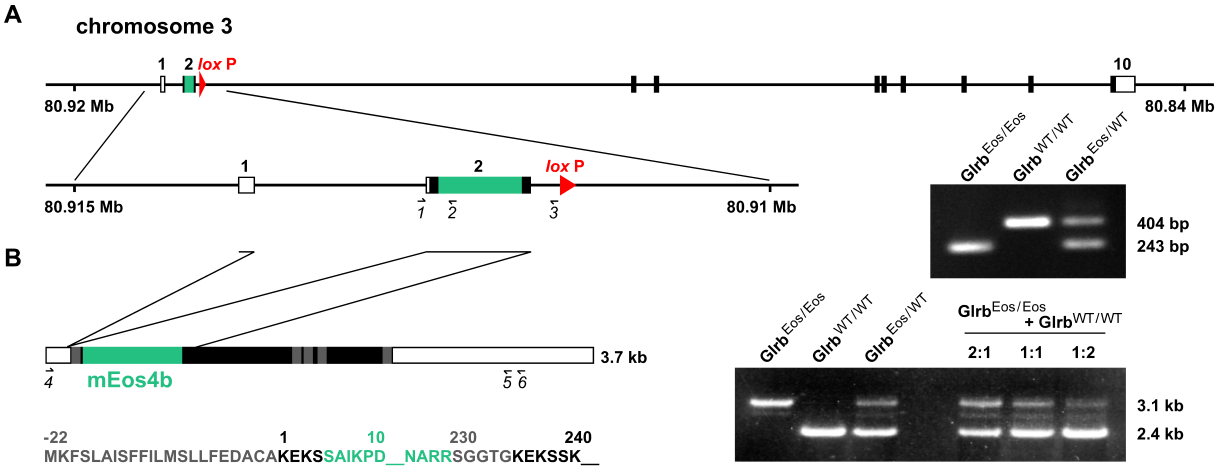

Fig. S1. Generation of the mEos4b-GlyRβ knock-in mouse model.

(A) The coding sequence of mEos4b (green) was inserted in exon 2 of the *Glrb* gene by homologous recombination, as shown by the amplification of a 243 bp PCR product in genomic DNA from *Glrb*$^{Eos/Eos}$ and *Glrb*$^{Eos/WT}$ animals using the primers *1*, *2* and *3*. (B) Splicing and transcript expression. The mEos4b sequence is inserted after the signal peptide (shown in gray) before the extracellular domain of the GlyRβ subunit. Right panel: Semi-quantitative RT-PCR. Mixing of spinal cord mRNA from *Glrb*$^{Eos/Eos}$ and *Glrb*$^{WT/WT}$ animals at a 1:1 ratio and amplification with primers *4* and *5* produces a PCR pattern that matches the amplification of the two alleles from the heterozygous *Glrb*$^{Eos/WT}$ mRNA.

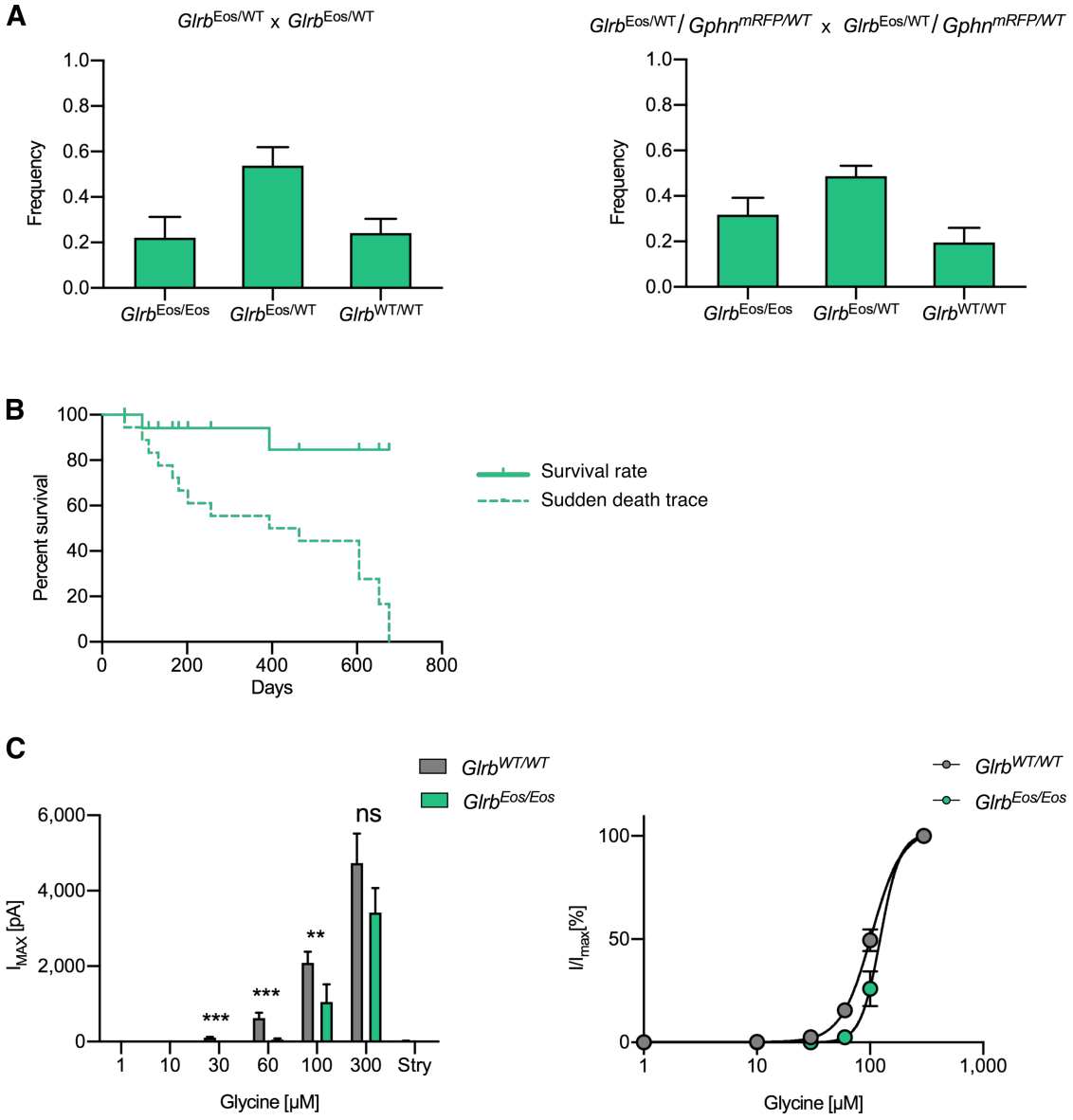

Fig. S2. Physiological and functional characterization of mEos4b-GlyRβ knock-in mice. (A) Mendelian inheritance of *Glrb*$^{Eos/Eos}$, *Glrb*$^{Eos/WT}$ and *Glrb*$^{WT/WT}$ genotypes in the offspring of heterozygous single KI matings *Glrb*$^{Eos/WT}$ x *Glrb*$^{Eos/WT}$ (left panel), and heterozygous double KI matings *Glrb*$^{Eos/WT}$/*Gphn*$^{mRFP/WT}$ x *Glrb*$^{Eos/WT}$/*Gphn*$^{mRFP/WT}$ (right panel). Left panel: N =42 pups from 5 litters, plot shows mean ± SEM; right panel: N = 45 pups from 7 litters. (B) Survival plot of homozygous knock-in mEos4b-GlyRβ mice (*Glrb*$^{Eos/Eos}$). N = 19 mice. (C) Left panel: Comparison of mean maximal currents (I_{max}) at different concentrations of glycine (1-300 µM) for *Glrb*$^{WT/WT}$ (N = 10) and *Glrb*$^{Eos/Eos}$ (N = 11 neurons). Glycinergic currents were blocked with 10 µM strychnine (Stry) at the end of each recording. Right panel: Normalized dose response curves for *Glrb*$^{WT/WT}$ and *Glrb*$^{Eos/Eos}$ show a subtle shift in the EC_{50} of mEos4b-GlyRβ containing receptors compared to the wild type. Plots show mean ± SEM. **p < 0.01, ***p < 0.001.

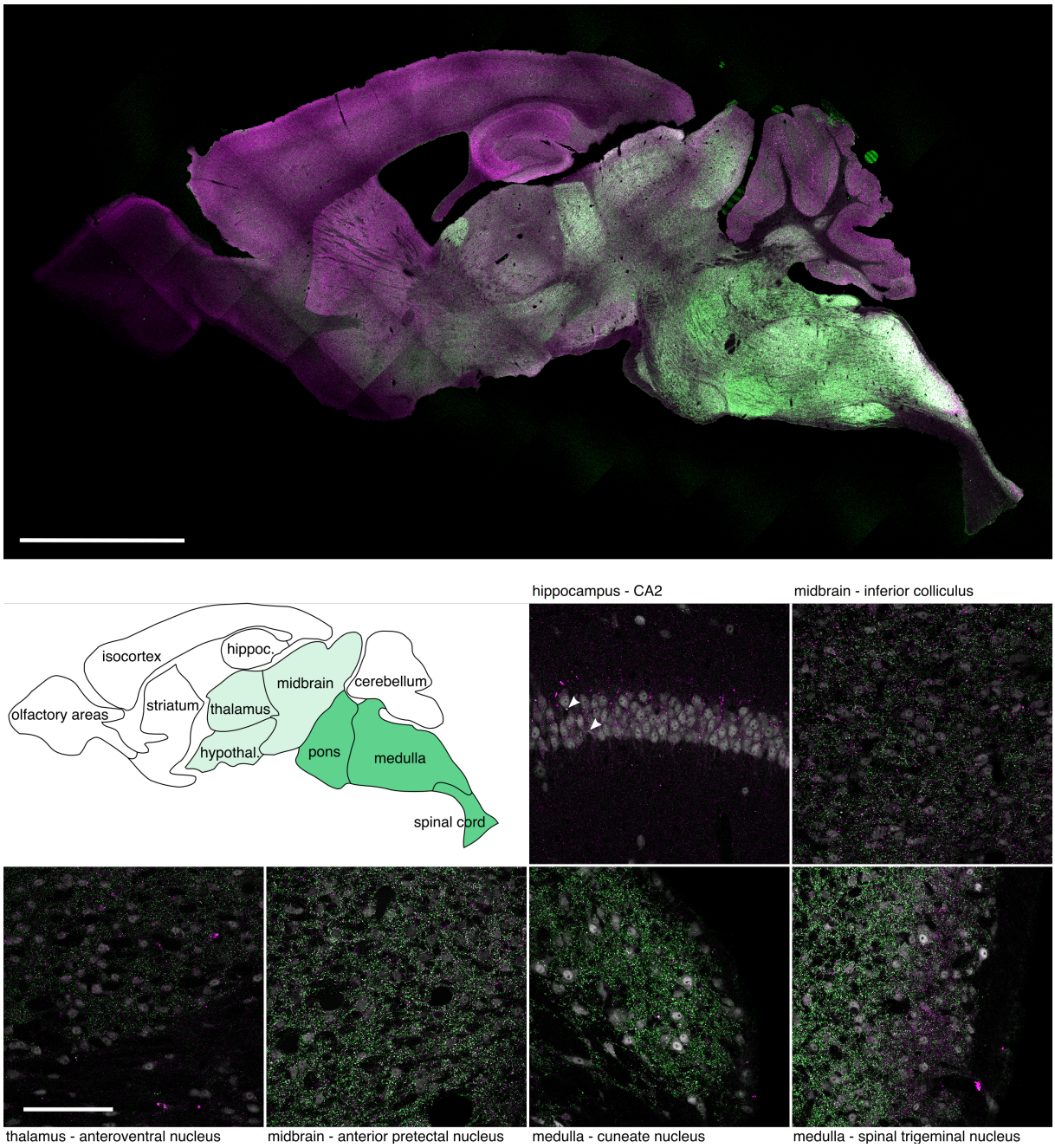

Fig. S3. Protein expression of mEos4b-GlyRβ in brain sections of knock-in mice.

Expression of mEos4b-GlyRβ (green) and mRFP-gephyrin (magenta) across brain regions (confocal image of a sagittal vibratome section of a double knock-in *Glrb*$^{Eos/Eos}$ / *Gphn*$^{mRFP/mRFP}$ mouse at 2 months of age). Scale bar = 2.5 mm. The brain atlas depicts the various brain regions with reference to the overall mEos4b-GlyRβ expression levels (white = none-low expression, light green = medium expression, darker green = high expression). High magnification images: Confocal images of various brain regions from the same vibratome section, showing the expression of mEos4b-GlyRβ (green) and mRFP-gephyrin (magenta), as well as NeuN immunolabeling (grey). Arrowheads depict synaptic puncta in the pyramidal cell body layer of the hippocampus that are positive for mEos4b-GlyRβ. Scale bar = 100 µm.

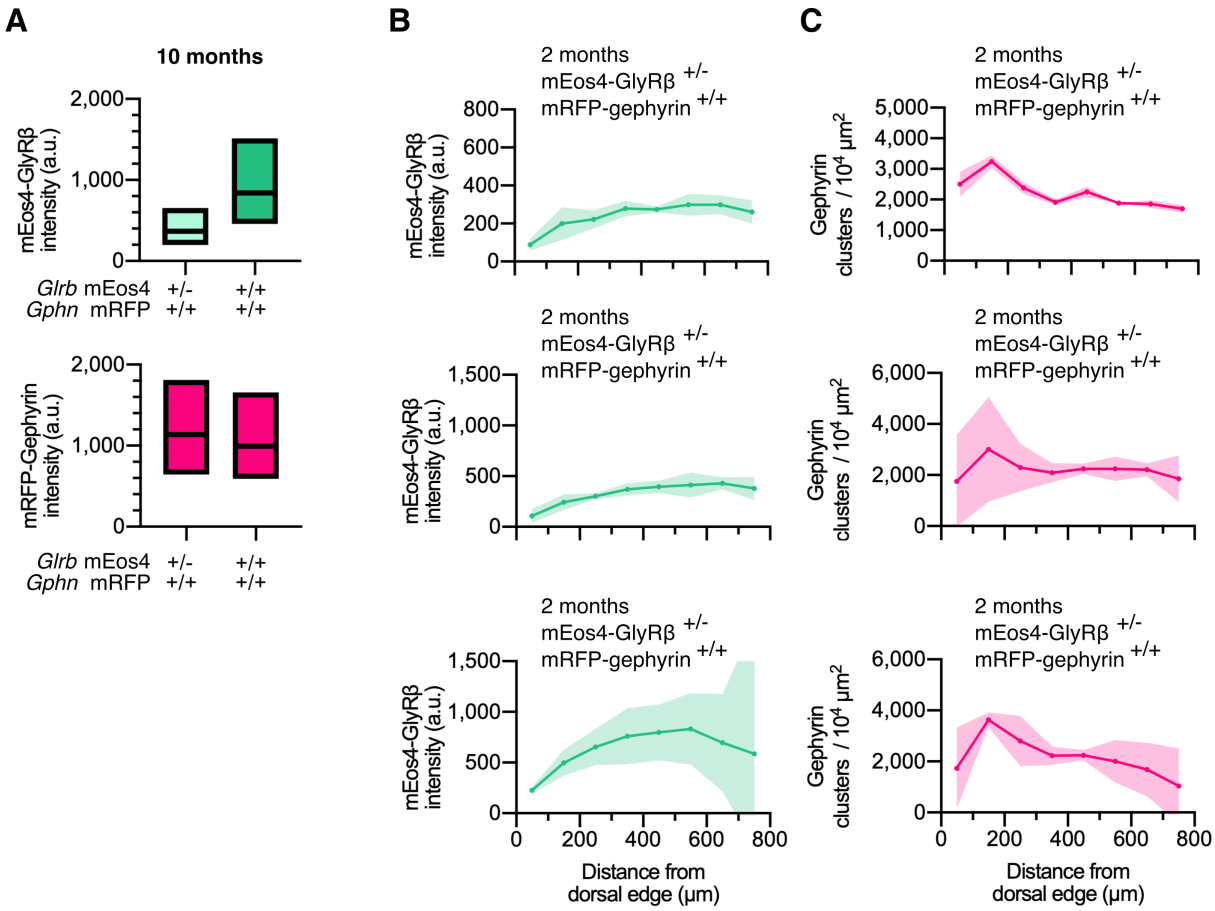

Fig. S4. Quantitative confocal imaging in 10 month old animals.

(A) Intensity of mEos4b-GlyRβ and mRFP-gephyrin at spinal cord synapses in homozygous and heterozygous mEos4b-GlyRβ mice, measured in the area indicated by the white square in Fig. 1A. Plots show median and quartiles. N = 5 images per condition from 5 tissue slices per genotype from 2 mice per age group. (B) Quantification of mEos4b-GlyRβ intensity at gephyrin-positive puncta across the spinal cord in 2 month old heterozygous (+/-; $Glrb^{Eos/WT}$) and 10 old month homozygous (+/+; $Glrb^{Eos/Eos}$) and heterozygous animals. Intensities measured in regions as indicated by rectangle in (Fig.1.A). Plots show mean ± 95% confidence interval. N = 2-4 images from 2-4 tissue slices from 2 mice per genotype. (C) Quantification of numbers of gephyrin clusters across the spinal cord in 2 month old heterozygous and 10 month old homozygous and heterozygous animals. Plots show mean ± 95% confidence interval. N = 2-4 images from 2-4 tissue slices from 2 mice per genotype.

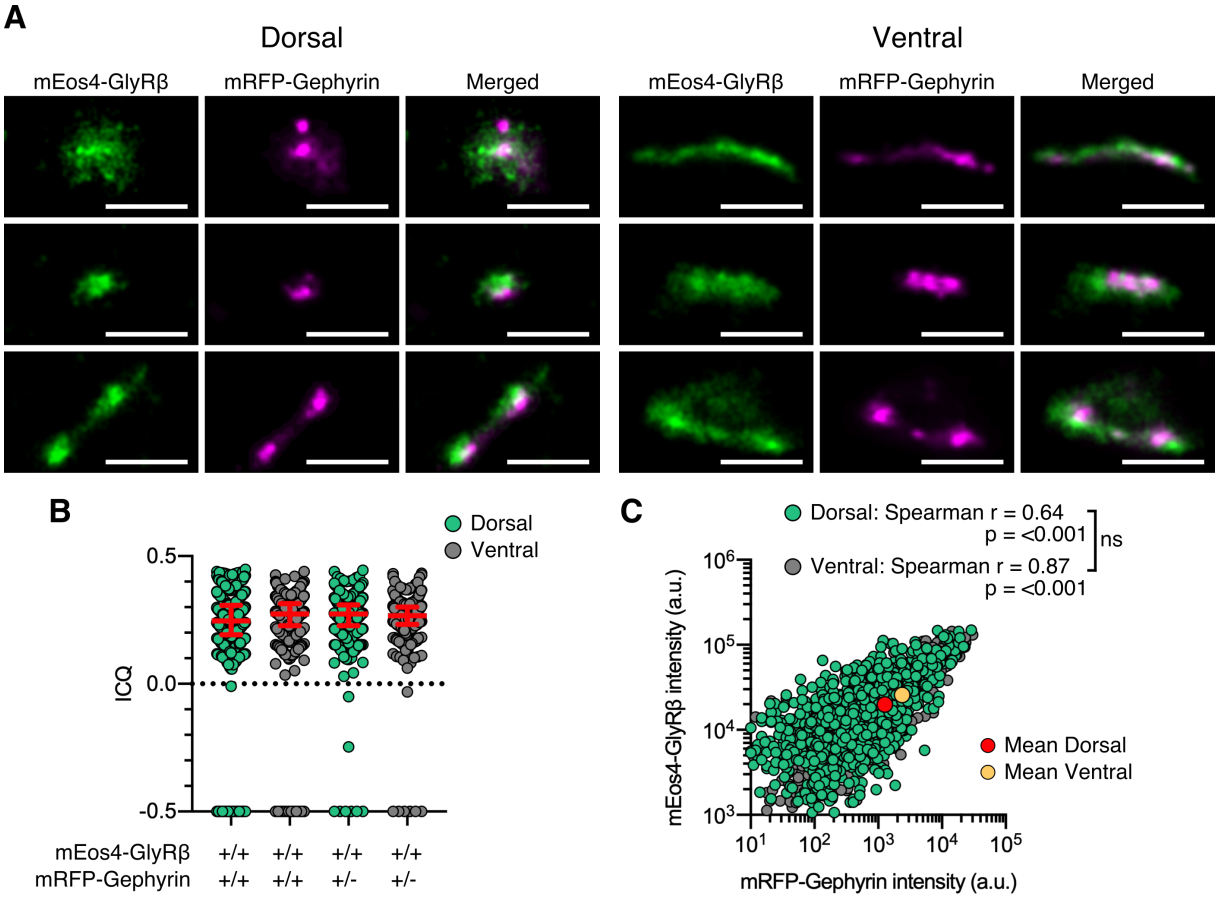

Fig. S5. Dual-color super-resolution synapse shape & 10 month correlation analysis.

(A) Examples of synapse shapes and sizes in dorsal and ventral tissue. Scale bar = 500 nm. (B) Intensity correlation quotient (ICQ) of mEos4b-GlyRβ and mRFP-gephyrin in 10 month old heterozygous and homozygous mice. Plot shows median ± interquartile range. N = 466-611 synapses from 17 dorsal and 19 ventral images from 7 tissue slices per spinal cord region from 2 mice per condition. (C) Quantification of GlyR-gephyrin occupancy in 10 month old homozygous mice (*Glrb*$^{Eos/Eos}$ / *Gphn*$^{mRFP/mRFP}$). Non-parametric Spearman's rank shows the same positive correlation at dorsal and ventral synapses. N = 1241 dorsal synapses and 813 ventral synapses. ns = not significant.

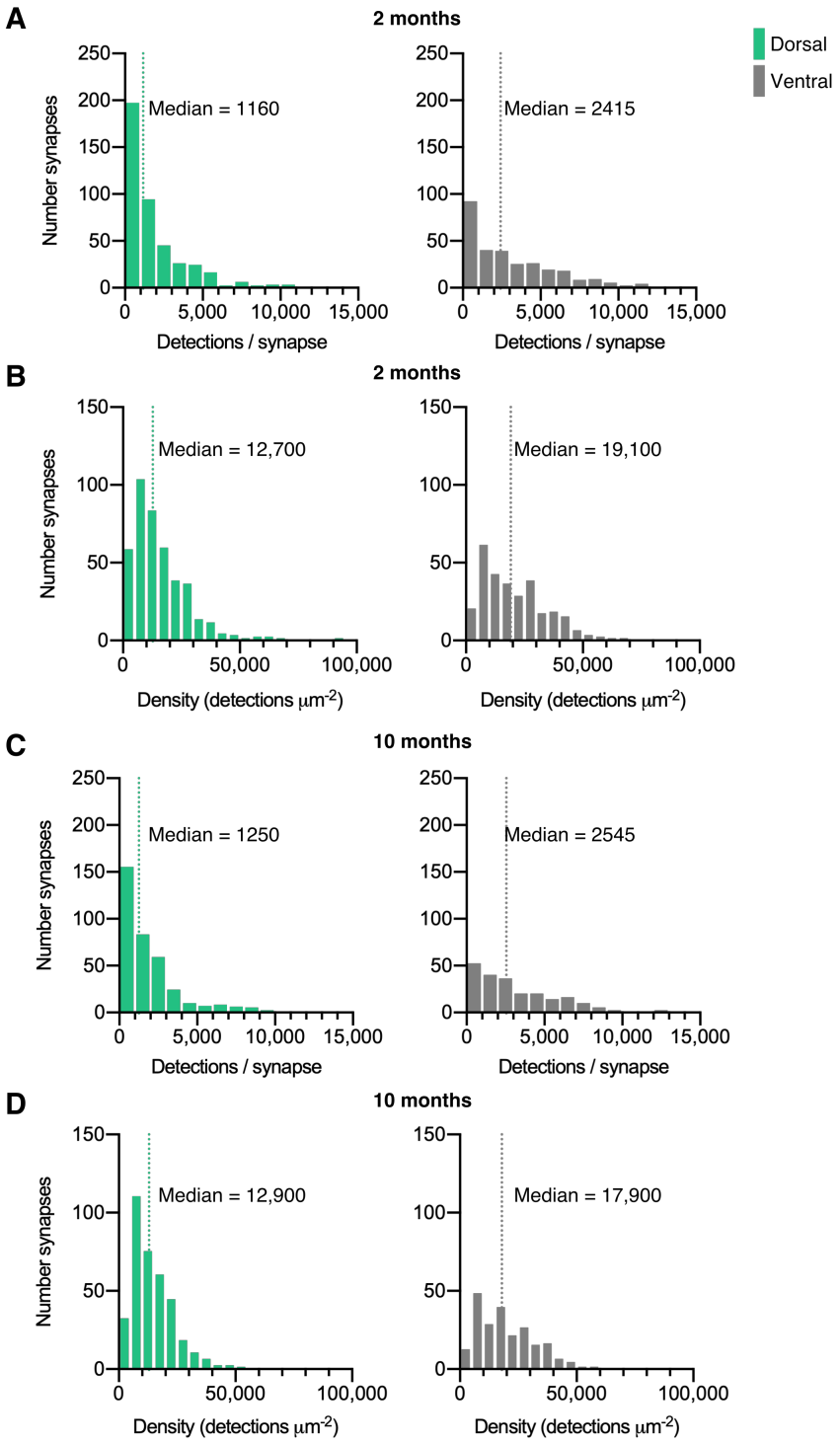

Fig. S6. Quantification of mEos4b detections at synapses.
Histograms of mEos4b-GlyRβ detections per synapse (A & C) and density of detections (B & D). N = 433 dorsal synapses and 304 ventral synapses in 2 month old mice. N = 372 dorsal synapses and 234 ventral synapses in 10 month old mice.

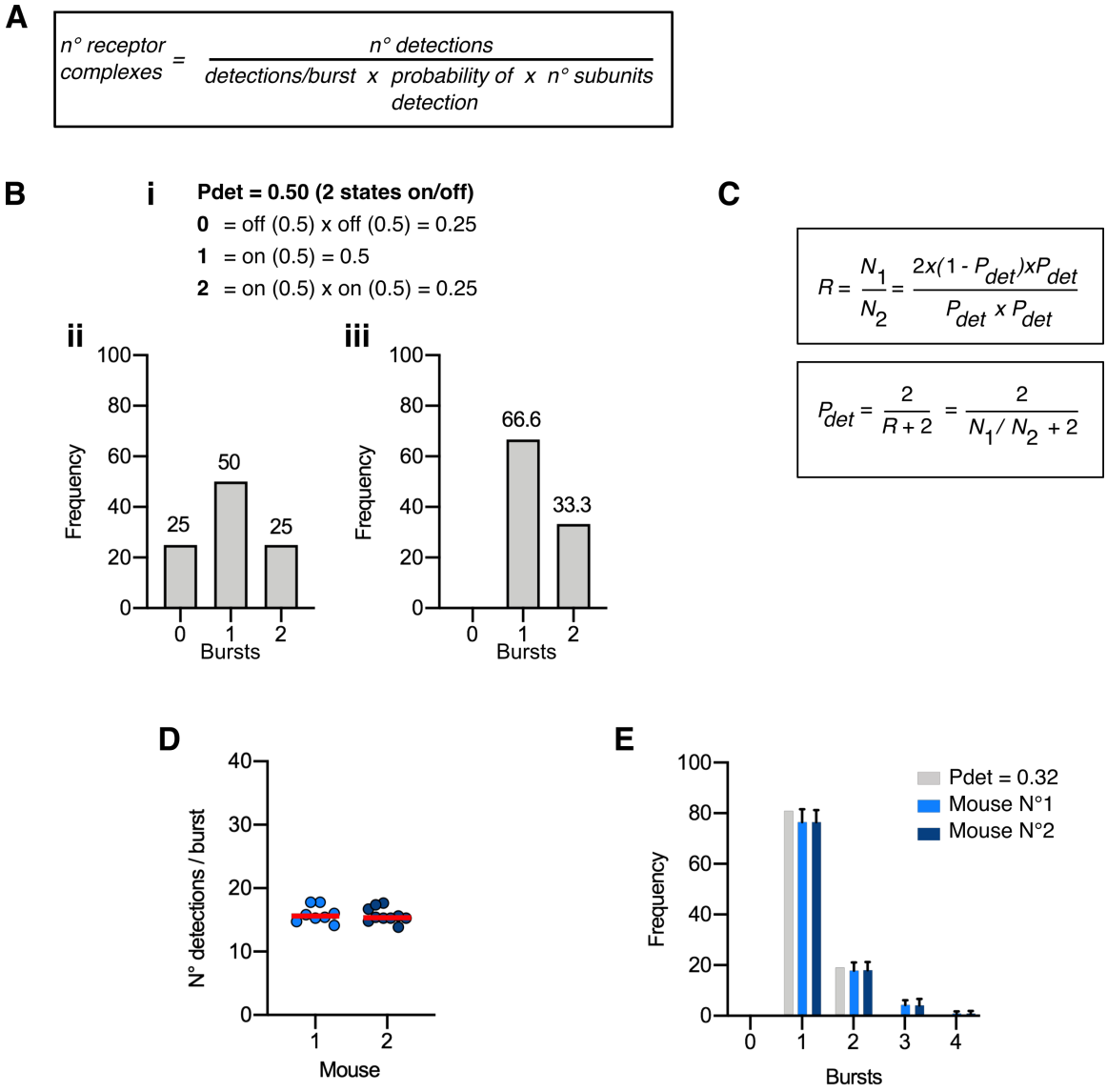

Fig. S7. Molecule conversion of mEos4b-GlyRβ detections into GlyRs copy numbers. (A) Descriptive formula for converting fluorophore detections into molecule numbers based on SMLM recordings in sparsely populated, extrasynaptic membrane compartments (Patrizio et al., 2017). Three parameters are required: the number of repetitive detections of the single fluorophores (average detections per burst), the probability that the fluorophore is functional (the probability of detection P_{det}), and the stoichiometry of the heteropentameric GlyR complex based on a α3:β2 receptor stoichiometry (Durisic et al., 2014, Patrizio et al., 2017). (B) Theoretical binomial distribution of the number of bursts of fluorescently labeled GlyRβ subunits (imaging 0, 1 or 2 subunits) and a $P_{det} = 0.5$ (i, ii), adjusted for the experimental situation in which only the counts of 1 and 2 bursts per cluster are visible (iii). (C) Derivation of the formula for calculating P_{det}, using the counts of 1 and 2 bursts of detections. (D) Number of mEos4b detections per burst in homozygous *Glrb*$^{Eos/Eos}$ animals from our experimental data. N = 8-9 images per mouse from 2 mice. (E) Distribution of the number of bursts of mEos4b detections in homozygous *Glrb*$^{Eos/Eos}$ mice. N = 8-9 images per mouse from 2 mice. The light gray bars represent the adjusted distribution for $P_{det} = 0.32$ that was calculated from the experimental data (blue bars) according to the formula given in (C).

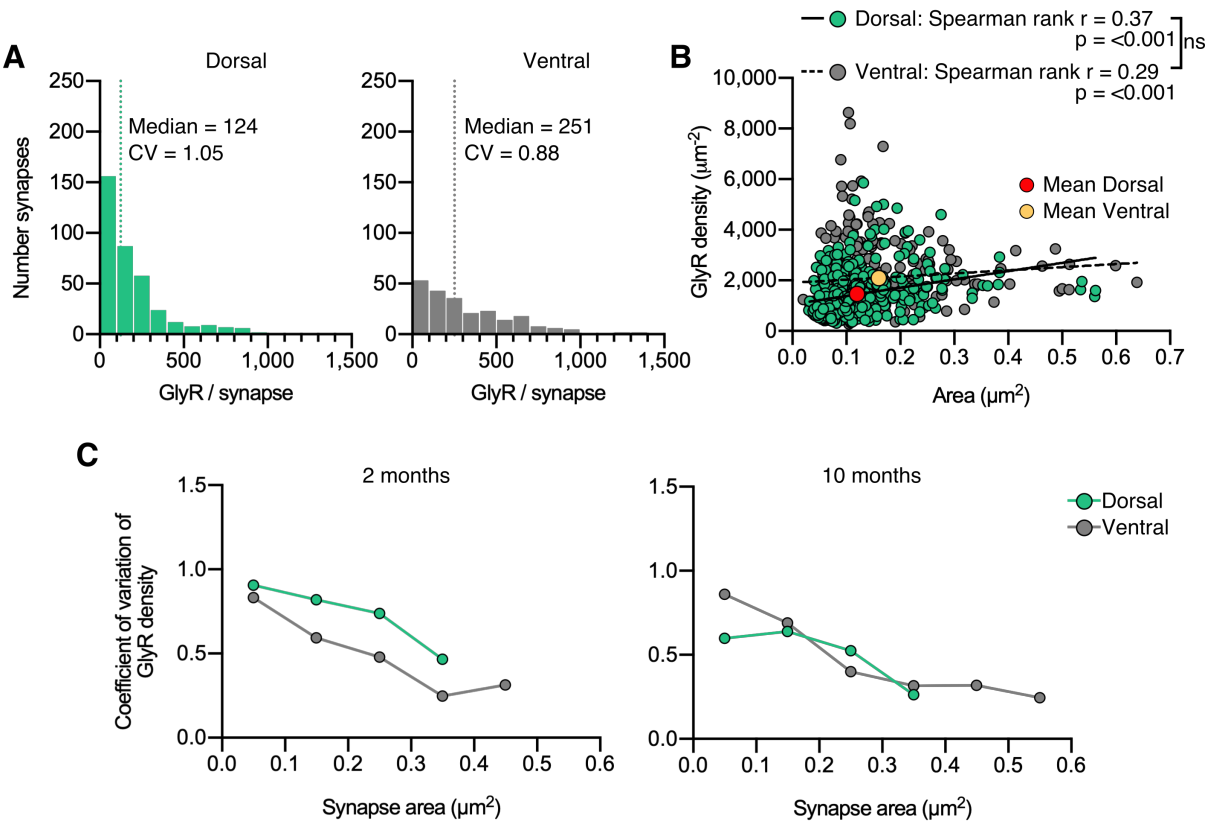

Fig. S8. Copy numbers and GlyRs densities at synapses (10 months).
(A) Histogram of the number of GlyRs per synapse calculated from the molecular conversion of detections in 10 month old mice (see Fig. S6 and S7). N = 372 dorsal and 234 ventral synapses from 20 images from 7 tissue slices per region from 2 mice. CV = coefficient of variation. (B) Scatter plot of GlyR density vs synapse area shows no difference between dorsal and ventral synapse densities. ns = not significant. (C) Analysis of the coefficient of variation of GlyR density with respect to synapse area for dorsal and ventral synapses in 2 and 10 month old mice.

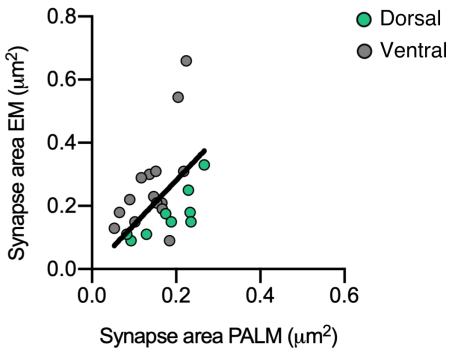

Fig. S9. Comparison of PALM and EM area measurements.
Comparison of synapse areas measured by PALM and EM shows a close correspondence.

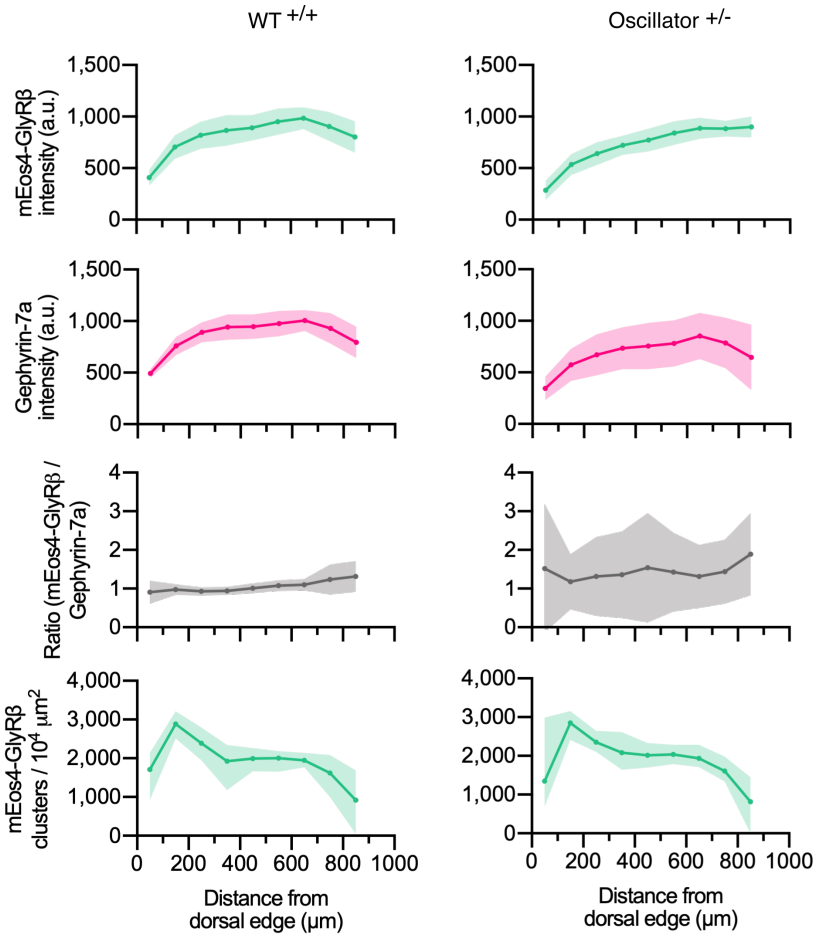

Fig. S10. Quantitative confocal analysis at mEos4 puncta of the *oscillator* mouse model. Intensity of mEos4b-GlyRβ and mRFP-gephyrin at mEos4-positive puncta across the spinal cord in mice heterozygous (+/-) for oscillator compared to homozygous WT (+/+) littermates. All mice are homozygous for mEos4b-GlyRβ. Intensities measured in regions as indicated by rectangle in (Fig.1.A). Plots show mean ± 95% confidence interval. N = 9-11 images from 9-11 tissue slices from 2 mice per genotype (same data as in Fig. 4, but using a mask generated in the mEos4b channel instead of the Cy3 immunolabeled gephrin).

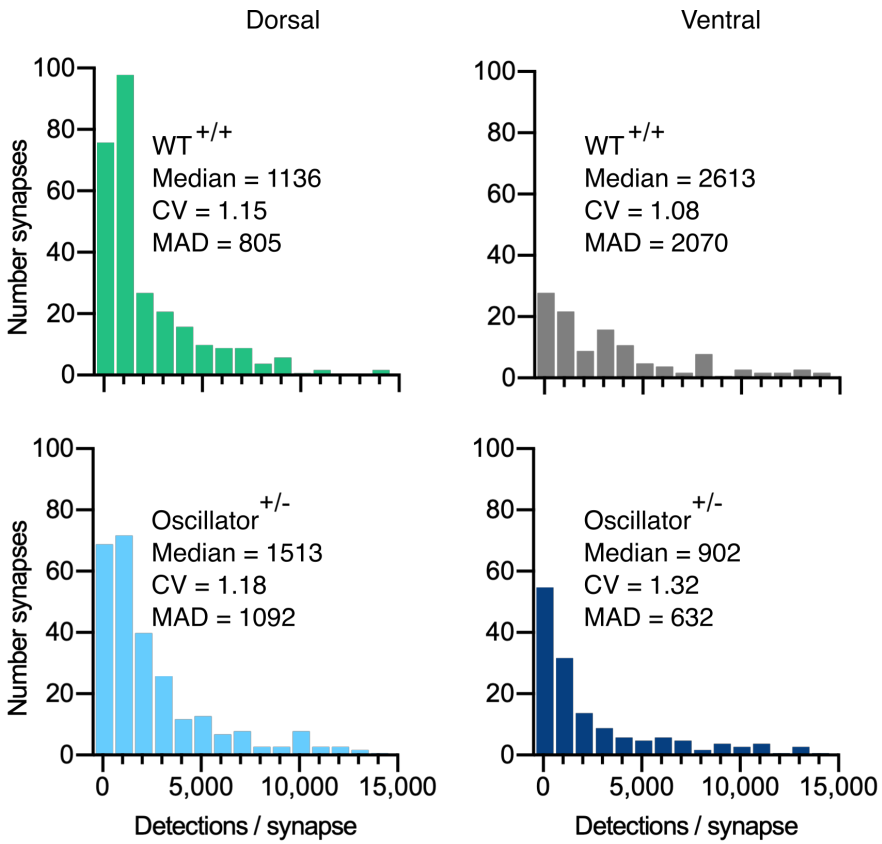

Fig. S11. Quantification of mEos4b detections at synapses in the *oscillator* mouse model. Histograms of mEos4b-GlyRβ detections per synapse in heterozygous (+/-) *oscillator* and homozygous (+/+) WT littermates. N = 282 WT dorsal and 120 ventral synapses, 273 *oscillator* dorsal and 156 ventral synapses from 2-4 tissue slices and 2 mice for all conditions. CV = coefficient of variation, MAD = median absolute deviation.

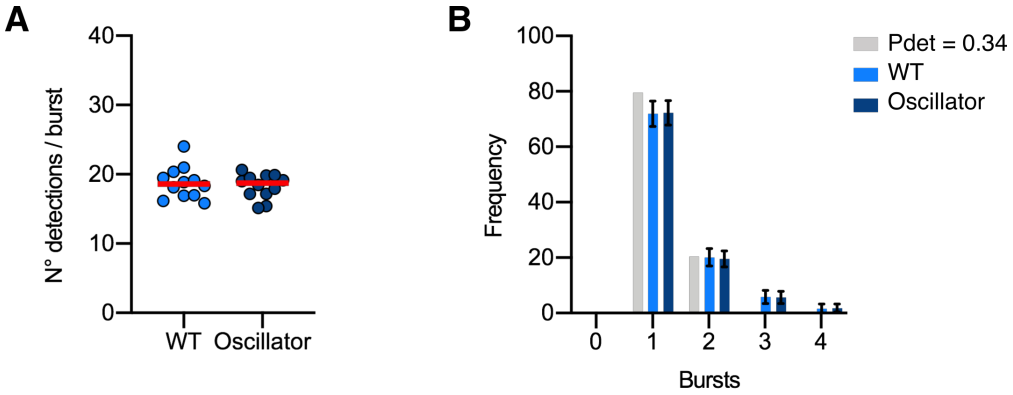

Fig. S12. Molecule conversion of mEos4b-GlyRβ detections into GlyRs copy numbers in the oscillator mouse model.
(A) Number of mEos4b detections per burst in homozygous *Glrb*$^{Eos/Eos}$ mice in heterozygous *oscillator* and homozygous WT littermates. N = 12 images per mouse. (B) Frequency distribution of bursts of mEos4b detections in homozygous *Glrb*$^{Eos/Eos}$ mice. The light gray bars indicate a binomial distribution for P_{det} = 0.34 that was calculated from the experimental data as described in Fig. S7. N = 12 images per mouse.